

ANALYZING AND VISUALIZING COSMOLOGICAL SIMULATIONS WITH PARAVIEW

JONATHAN WOODRING¹, KATRIN HEITMANN², JAMES AHRENS¹, PATRICIA FASEL³, CHUNG-HSING HSU⁴, SALMAN HABIB⁵, AND ADRIAN POPE^{2,5}

¹ CCS-7, CCS Division, Los Alamos National Laboratory, Los Alamos, NM 87545

² ISR-1, ISR Division, Los Alamos National Laboratory, Los Alamos, NM 87545

³ CCS-3, CCS Division, Los Alamos National Laboratory, Los Alamos, NM 87545

⁴ Oak Ridge National Laboratory, Oak Ridge, TN 37831 and

⁵ T-2, Theoretical Division, Los Alamos National Laboratory, Los Alamos, NM 87545

Submitted to the Astrophysical Journal Supplements

ABSTRACT

The advent of large cosmological sky surveys – ushering in the era of precision cosmology – has been accompanied by ever larger cosmological simulations. The analysis of these simulations, which currently encompass tens of billions of particles and up to trillion particles in the near future, is often as daunting as carrying out the simulations in the first place. Therefore, the development of very efficient analysis tools combining qualitative and quantitative capabilities is a matter of some urgency. In this paper we introduce new analysis features implemented within ParaView, a parallel, open-source visualization toolkit, to analyze large N -body simulations. The new features include particle readers and a very efficient halo finder which identifies friends-of-friends halos and determines common halo properties. In combination with many other functionalities already existing within ParaView, such as histogram routines or interfaces to Python, this enhanced version enables fast, interactive, and convenient analyses of large cosmological simulations. In addition, development paths are available for future extensions.

Subject headings: methods: numerical — cosmology: large-scale structure of universe

1. INTRODUCTION

During the last two decades, cosmological measurements and predictions have advanced from the level of estimates to precision determinations – at better than the 10% level – of the major cosmological parameters. In the next decade, ongoing and upcoming surveys such as the Sloan Digital Sky Survey III, PanStarrs, the Dark Energy Survey, the Large Synoptic Survey Telescope, the Joint Dark Energy Mission, or Euclid, to name a few, promise improvements in the measurement state of the art by yet another order of magnitude. At the same time, theoretical predictions at the same or better levels of accuracy are needed to fully exploit the information available from these surveys. Predictions of this quality can only be obtained by high-performance simulations which cover cosmological volumes representative of those observed by the surveys. At the same time, the simulations must possess high enough mass and force resolution to reliably resolve dark matter halos which host galaxies. For gigaparsec cubed volumes, the requirements translate to tens to hundreds of billions of simulation particles.

In the past several years, this simulation challenge has been attacked from different perspectives. A few ‘hero’ simulations have been carried out: The Millennium simulation from 2005 with ~ 10 billion particles and the two ‘Horizon’ simulations from 2009 with ~ 70 billion particles each (Teyssier et al. 2009; Kim et al. 2009), but with lower force resolution, are prominent examples. Another approach is to run more moderately sized simulations (still one to ten billion particles each) but with many realizations and different volumes for one cosmological model. This allows for efficient gathering of statistics and the determination of covariances (e.g. the LasDamas Project by McBride et al. (2010) and the MICE simulations by Crocce et al. 2010). Such simulations can also be carried out for different cosmologies (e.g. the Coyote Universe by Heitmann et al. 2010, 2009; Lawrence et al. 2010) to explore

the cosmological parameter space and derive predictions for different statistics of interest. Both approaches generate a large amount of data and the analysis task is often as demanding as carrying out the simulations themselves. It is therefore very desirable to develop efficient, flexible, versatile, and easily extendable tools to help with the analysis task. Taking this thought one step further, an analysis tool that combines quantitative and qualitative features would be particularly convenient; such a tool should allow visualization and analysis of the data at the same time, and allow user-customizable features and extensions.

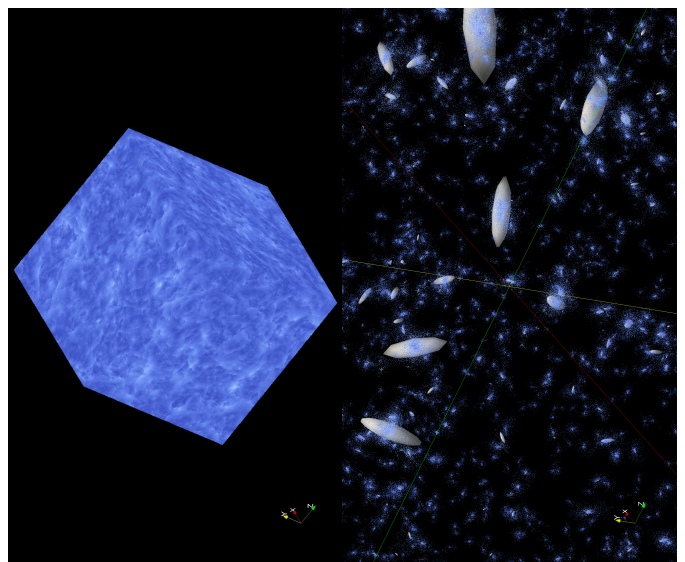


FIG. 1.— ParaView visualization of a billion particle simulation from the Coyote Universe suite (Lawrence et al. 2010). Left: visualization of all particles colored by their velocities; right: visualization of a sub-volume showing particles in halos and the halo centers.

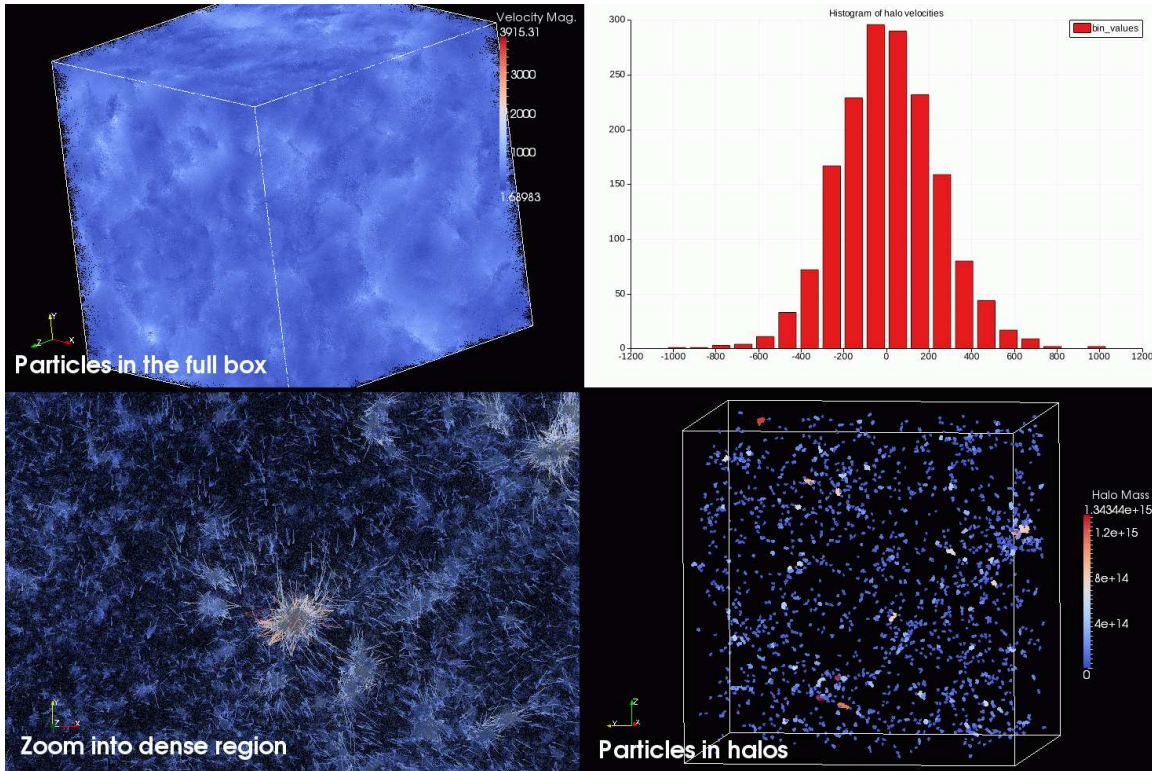


FIG. 2.— Examples of different analysis capabilities of ParaView. The simulation shown here is described in Section 3.1. The upper left panel shows all the particles in the box colored with respect to their velocities, the lower left panel shows a zoom-in into a dense region. The upper right panel shows a histogram of halo velocities. The lower right panel shows only the particles that reside within halos.

Over the last several years we have developed a visualization and analysis tool based on ParaView, an open-source, parallel visualization framework. Figure 1 shows an example visualization of a billion particles carried out on 128 processors. We used ParaView for some of the analyses carried out in Heitmann et al. (2008). In Hsu et al. (2010) we demonstrated the tool’s efficiency for scientific investigations by analyzing the formation of halos over time. In the current paper, we introduce the new features we have implemented into ParaView to analyze and visualize large cosmological N -body simulations. These features are included in the latest ParaView 3.8 release¹. ParaView is a very convenient platform for several reasons: (i) it is parallel and therefore well suited for very large data sets, (ii) some general data analysis routines already exist within it, (iii) it is open source, and (iv) it can be coupled with relative ease to existing codes and includes interfaces to programming languages, e.g., Python.

We have implemented two different particle readers into ParaView, one based on the ‘cosmo’ format introduced in Heitmann et al. (2005), the other following the ‘GADGET’ format² widely used by the cosmology community and the native data format of the cosmology code GADGET-II (Springel 2005). The cosmo format is a simple binary format for storing particle positions, velocities, tags, and mass. The GADGET format allows for more flexibility and information, although currently the ParaView reader only reads the N -body particles from the GADGET files. A future ParaView release will include the option of reading gas information as well. In addition to the readers, we have implemented a very efficient

parallel halo finder that supports the friends-of-friends (FOF) algorithm. Combined with the analysis features already available, such as histogram routines, density routines, comparative visualization, movie options and so on, ParaView provides a convenient and flexible visualization and analysis environment.

The paper is organized as follows. First, we give a short overview of ParaView and briefly describe the new cosmology modules that have been implemented. In Section 2.2.1 we provide a more detailed description of the parallel halo finder and the halo properties available. We give an example for how ParaView can be used to analyze cosmological simulations in Section 3 and conclude in Section 4. We give a brief introduction on the ParaView GUI and the use of the cosmology filter in the Appendix.

2. PARAVIEW

ParaView (Ahrens et al. 2005) is a general-purpose, open-source, scientific visualization server technology built on top of VTK (the Visualization Toolkit) (Schroeder et al. 1996). Through the ParaView server, visualization of large-scale data is possible by parallelism and data streaming on a scalable server backend. The default ParaView application runs a built-in single-threaded ParaView server for small visualization tasks. For larger data, it can connect to a remote Message Passing Interface (MPI) parallel ParaView server backend that is running on a visualization cluster or parallel supercomputer.

The process of visualization within ParaView consists of constructing VTK visualization pipelines of readers and filters, where outputs are implicitly connected to render views. Readers allow data to be imported into the pipeline, while filters allow data to be analyzed and manipulated through pro-

¹ <http://www.paraview.org/>

² <http://www.mpa-garching.mpe.de/GADGET/users-guide.pdf>

cessing. Render views provide visual representations of data that a user can interact with. Visualization pipelines are constructed through a front-end interface, which is capable of communicating with the ParaView server, and are executed on the data by the server. Visual results are displayed by the front-end from images or geometry sent back by the ParaView server after processing data using a constructed visualization pipeline.

A variety of tools and languages can interface with the ParaView server backend to analyze and visualize data. The images we show in the following were created using the default ParaView graphical user interface client available from the ParaView website. The default ParaView GUI is a Qt application, with Python scripting support, that is available on Windows, OS X, Linux, and on any other platform that is able to compile C++ code with the Qt framework (Summerfield 2010). ParaView is also capable of performing visualization and analysis through other front-ends, such as task specific visualization tools built on top of the ParaView server language bindings in Python, Tcl/Tk, C++, Java, and Javascript. The ParaView parallel server backend compiles on any platform capable of compiling C++ and MPI code. Information on using ParaView and downloading source and binaries is located at paraview.org.

2.1. Parallel Reading

Assuming that the ParaView server is running in parallel (the reader will work in serial mode as well), the first task to visualize cosmology data is to correctly read the data and distribute it among the processors. The ParaView reader we have implemented for the “cosmo” format has also been extended to work with the “GADGET” format (for N -body particles). Particle files can be single monolithic files or multiple files generated per-processor during the simulation.

The first task the reader performs is assignment of processors to regions in space, such that a processor will be assigned a contiguous block in space. We use a three dimensional spatial decomposition. Each processor will eventually obtain all of the particles in that space. The second task is reading the particle file or files. If there is a single file, all of the processors will read into memory a linear portion of the particle list, temporarily taking ownership of the particles in that segment of list. Likewise, if there are per process files, each processor will read a file assigned to it, and take temporary ownership of the particles located in that file. If there are fewer or more files per process, the files are divided such that each processor reads an equal number of particles.

Next, processors take ownership of the actual particles that belong to them through communication of particles, i.e., moving the particles to the correct processor that owns the spatial region containing the particle. In the first step, the processors examine the particles currently in memory and separate out the particles that belong on that processor, from the particles that do not belong. Next, all of the processors simultaneously send a buffer of particles that do not belong to the next rank processor, while receiving a buffer from the previous rank processor. Each processor will examine the buffer received and take out the particles that belong to it. If the number of files is greater or equal the number of processors, this process is repeated for $p - 1$ rounds, where there are p processors, until all of the particles are in memory on the correct processor. In the case of more processors than files, the round robin circles are smaller so that every processor reads a file if possible. For example, for 16 files and 64 processors,

4 processors will read each file and the round robin chain is $[(p/4) - 1]$ in size.

Finally, in order to perform correct halo finding per-process, we allow for spatial overlap in the per-process volumes and duplicate the particles across overlap regions. Given that the entire space is divided into blocks and there is wraparound on boundaries (because of periodic boundary conditions), each processor will have 26 neighbor processors. With an appropriate overlap boundary size, as explained in Section 2.2.1, each processor can determine the volume overlap or intersection regions with its neighbors. The duplicate or “ghost” particles in the overlap regions are communicated to each of spatially contiguous neighbor processes to expand the volume of each process.

2.2. Parallel Filtering and Rendering

The data, as it is read in, is treated as a parallel VTK unstructured point data set in the visualization pipeline. The “cosmo” format provides point position, velocity, mass, and a tag available as data attributes (fields, or variables) per point in a binary file. The data at this point can be rendered as is, using parallel point rendering colored by data attribute, or it can be analyzed and manipulated through various parallel VTK filter modules before rendering.

There are many built-in VTK filters available in ParaView, and it takes a small amount of effort by an expert user to expose an existing VTK filter in ParaView that is not already available by default. It involves creating an XML plugin to tell ParaView how to interface with the VTK internals. Some useful filters available by default in ParaView are the Calculator, Threshold, and Glyph filters. The Calculator filter allows new derived fields to be calculated on the fly from existing scalar, vector, and tensor fields using a mathematical expression. The Threshold filter discards data points that do not lie within a given range for a data value. The Glyph filter generates new geometry per point that can be scaled and oriented by attributes, such as spheres whose size is dependent on mass or arrows that point in the direction of the velocity and scaled by the velocity magnitude. Examples are shown in Section 3. Finally, if a desired filter does not already exist in VTK, ParaView includes the capability to script new filters in Python.

2.2.1. An Efficient, Parallel, Friends-of-Friends Halo Finder

An important component of the new ParaView cosmology capabilities is a very efficient parallel halo finding filter. The base implementation is a fast serial FOF halo finder, with parallel integration added. For finding FOF halos, the user can specify the linking length and the minimum number of particles defining a halo. ParaView returns a halo catalog containing halos with average position, average velocity, one-dimensional velocity dispersion, and mass for each halo. Optionally, the original particle list can be also be annotated with the halo information that each particle belongs to.

In order to achieve performance goals for the halo finding algorithm, we first developed a new serial halo finder (Hsu et al. 2010). A naive implementation of an FOF finder would check each and every particle pair; given n particles, therefore requiring $\mathcal{O}(n^2)$ operations, clearly an unacceptable scaling. To reduce the number of operations, we use a balanced kd-tree. A balanced kd-tree is a binary space partitioning data structure that organizes points in a k -dimensional space in such a way that the number of points in a subtree at each level are equal. Building a fully balanced tree from n points takes $\mathcal{O}(n \log n)$ operations.

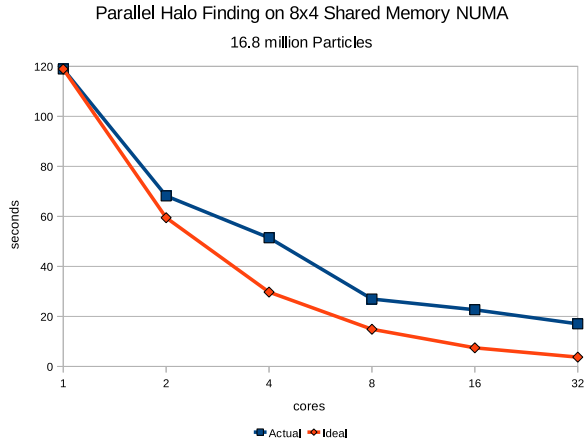


FIG. 3.— Strong scaling of the parallel halo finder in ParaView. The red curve shows ideal scaling, while the blue curve shows the actual timing. The problem size is fixed (256^3 particles) as the number of cores is increased from 1 to 32. Scaling is close to ideal; reasons for the departures are discussed in the text.

A recursive FOF algorithm starts at the leaf nodes (single particles) and merges nodes into halos by checking if the particles are within a given range of each other. As particles are merged into halos, particle tests are reduced by using subtree bounding boxes as proxies for points. If a subtree bounding box is too distant, all of the points can be skipped. Vice versa, if an entire bounding box is close enough all of the points can be added to a halo.

Once a fast serial FOF finder has been built, the next step is to implement efficient parallelization. We use a straightforward strategy by dividing the simulation volume into per-processor sub-volumes and allow these sub-volumes to overlap, as described in Section 2.1. The overlap length should be larger than the diameter of the largest halo, usually ~ 5 Mpc is a conservative choice. This is done to ensure that each halo is complete in at least one processor (overlapped) sub-volume. Next, the algorithm finds all halos in the sub-volumes. The last step is to ensure that each halo once is counted only once. When a halo is shared between two processors across a plane, it is assigned to the processor which has the halo in the upper plane (this is an arbitrary choice) and is eliminated from the other. If it is shared by more than one processor, the information is sent to an arbitration processor that makes the assignment and informs all other processors.

Strong scaling (execution time as a function of processor number with fixed problem size) of the halo finder is demonstrated in Figure 3. The test shown is carried out on a 32 core shared memory machine with 128 GB of RAM. The test used a 256^3 particle simulation snapshot at $z=0$. The actual timing of the halo finder is slightly higher than the ideal value, due to several reasons: (i) The halo finder is not fully load balanced since a large halo would cause a certain processor to do more work than others. For large volume simulations this is not a severe problem since not very many exceptionally large halos form. (ii) Due to the overlap strategy, the workload increases as parallelism increases. (iii) The ideal curve does not account for communication overhead. With these caveats in mind, the scaling behavior of the halo finder is very good. In addition, we also carried out a timing test on a 1024^3 particle simulation in distributed memory MPI. Results are given in Table 1.

TABLE 1
HALO FINDER TIMING FOR A BILLION PARTICLES

# of processors	Time in sec
64	66.6
128	32.9
256	20.5

Halos do not have a uniquely defined notion of ‘halo center’. Of the different possibilities, the center of mass is the easiest to implement and fastest to run. In this case, the particle-averaged position of the halo is given by

$$\mathbf{x}_{\text{FOF}} = \langle \mathbf{x} \rangle = \frac{1}{n_{\text{FOF}}} \sum_i^{n_{\text{FOF}}} \mathbf{x}_i, \quad (1)$$

where \mathbf{x}_i is the position of the i^{th} particle in the halo and n_{FOF} is the number of particles in the FOF halo. The halo center of mass velocity is determined in an analogous fashion. Because this is the fastest way of determining the halo center, it is the default setting we choose for ParaView. Of course this definition has obvious shortcomings: e.g., if a halo is comprised of two distinct subhalos, the center of mass will lie in between those subhalos and not at the center of the more massive subhalo. A more accurate determination of the halo center is therefore given by either finding the potential minimum of the halo or to find the particle with the most neighbors (these two centers are very close and for most halos in fact identical). In future, ParaView will allow for this option in addition to determining the center of mass.

In addition, the halo finder provides a measurement of the one-dimensional velocity dispersion, given by:

$$\sigma_v = \sqrt{\frac{1}{3} \left(\frac{1}{n_{\text{FOF}}} \sum_i^{n_{\text{FOF}}} \mathbf{v}_i \cdot \mathbf{v}_i - \mathbf{v}_{\text{FOF}} \cdot \mathbf{v}_{\text{FOF}} \right)}. \quad (2)$$

In future, the set of halo properties calculated by ParaView will be extended to include e.g. spherical overdensity mass and halo concentration as well as sub-halo finding. The current 3.8 release is limited to the aforementioned halo finding features and halo properties.

3. ANALYSIS OF COSMOLOGICAL SIMULATIONS WITH PARAVIEW

In this section we focus on a simple example to demonstrate how ParaView can be used to gain better intuition for cosmological structure formation by *visualizing* data sets and at the same time can be used to *analyze* the data sets and to extract quantitative information. The example we investigate is the effect of the force resolution in the simulation on the accuracy of halo masses.

The era of precision cosmology poses daunting challenges to theoretical cosmologists. Accuracy requirements at the 1% level for simulations of highly nonlinear processes such as structure formation demand extremely careful analyses of possible systematic errors in N -body simulations. A powerful probe of cosmology is the mass function which yields the number of halos as a function of their mass. The mass function is very sensitive to cosmological parameters and enables us to, e.g., distinguish between different models of dark energy. It was pointed out recently by Wu et al. (2010) and Cunha & Evrard (2010) that in order to analyze the data from

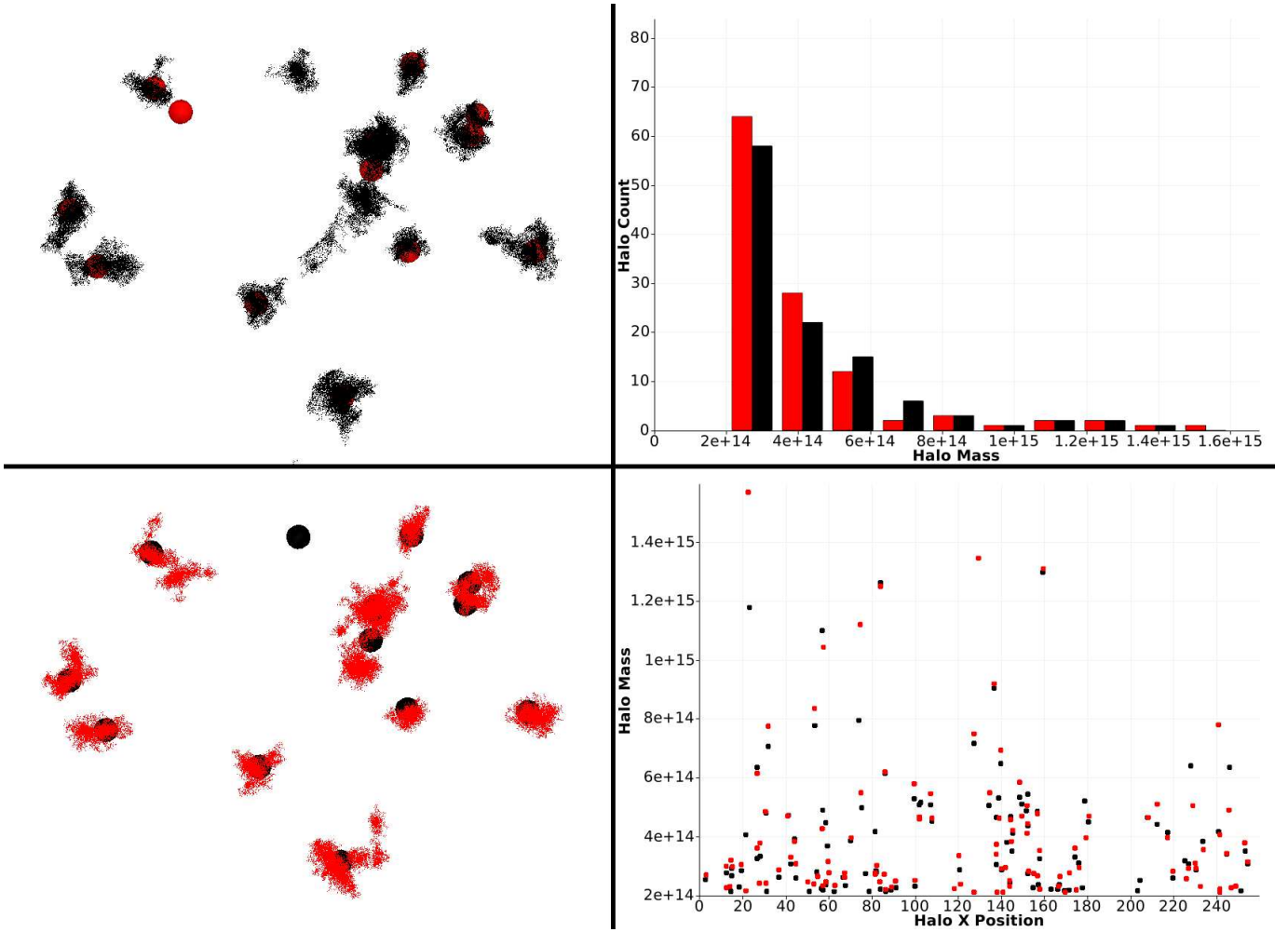


FIG. 4.— Force resolution and halo formation test: All results shown are for a linking length $b = 0.2$ and more than 3000 particles per halo. Results from the high resolution run are shown in red, results from the low resolution run are shown in black. Left upper panel: particles in halos from the low resolution run (black) and halo centers of halos from the low resolution run (red spheres) in a sub-volume of the simulation. The left lower panel has the same information but with particles from the high resolution run (red) and centers (black spheres) from the low resolution run. The overlinking problem can be seen for several halos: a very obvious example is a halo in the central region that links several structures together in the low resolution simulation. Also, the halos that are absent in the low resolution simulation are clearly at the lower mass end, the red centers in the upper left plot correspond to small halos that can be identified in the lower left plot. Note though, that these halos are not *missing* in the low resolution run, but rather not showing up in the plot because of our mass threshold of 3000 particles – in other words they are there but are below our mass threshold. Several points are apparent from this comparison: the low resolution halos are less concentrated, halos in the lower resolution run are more often overlanked, and some of the halos found in the higher resolution run are missing in the lower resolution run because they fell below the 3000 particle cut. The right upper panel shows a histogram of the halo counts as a function of mass. For the lowest two mass bins, the high resolution run has more halos than the low resolution run. The lower right panel shows the x -position versus halo mass, presenting the information in the two left panels in condensed, but more quantitative form. It also shows that the positions of the halos in both simulations are in reasonable agreement.

future cluster surveys we need predictions for the mass function at the 1% level of accuracy. Bhattacharya et al. (2010) find that uncertainties in the measurement of halo masses at the 2% level translate into inaccuracies in the mass function in the cluster mass regime at the 5-10% level. Therefore, understanding systematic biases of halo masses due to numerical shortcomings is a significant issue (aside from problems with the physical modeling itself) if we aim to predict the mass function at high accuracy.

Two major sources of numerical inaccuracy in determining halo masses are limitations in mass and force resolution. As pointed out by Warren et al. (2006), and later investigated by Lukić et al. (2007) for idealized Navarro-Frenk-White (NFW) halos (Navarro et al. 1997), undersampling halos with particles, i.e. insufficient mass resolution, leads to a systematic increase in the halo mass. The effect of insufficient force resolution is twofold: (i) The boundaries of the halo are not as

tight, therefore more particles from the surrounding area will be linked to the halo and lead to a mass increase. (ii) The concentration of the halo is considerably lower and less mass resides in the halo center, which can lead to a decrease in the total mass. We will use ParaView to investigate these force resolution effects in more detail and show how the use of ParaView can provide an intuitive understanding as well as yield quantitative results.

3.1. The Simulations

Our test analysis is based on a set of particle-mesh simulations, carried out with MC³ (Mesh-based Cosmology Code on the Cell), a new hybrid cosmology code that takes advantage of Cell-accelerated hardware (Habib et al. 2009; Pope et al. 2010). We investigate a Λ CDM model with the following cosmological parameters: $\omega_m = 0.1296$, $\omega_b = 0.0224$, $n_s = 0.97$, $\sigma_8 = 0.8$, and $h = 0.72$. We generate an

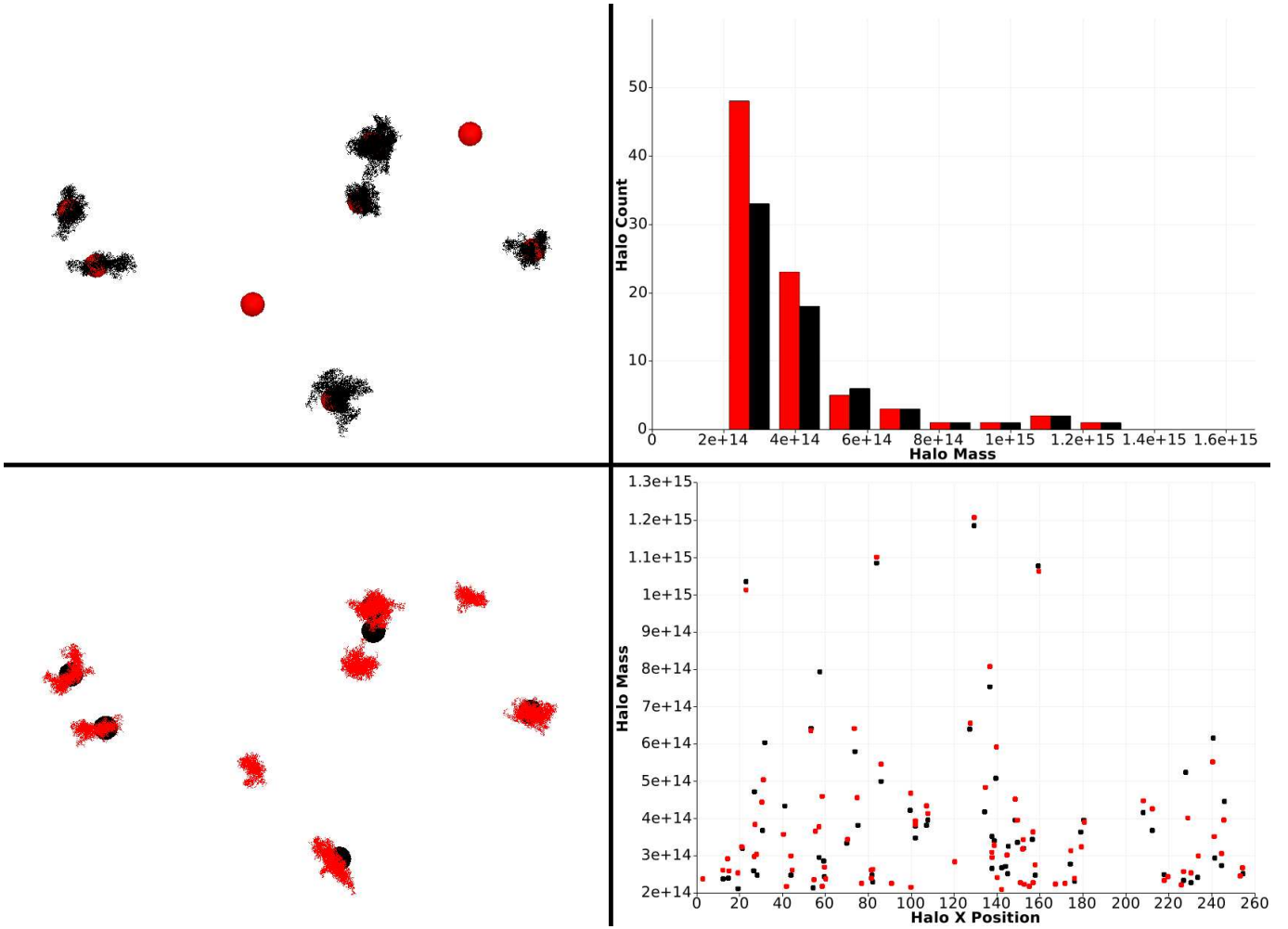


FIG. 5.— Same as in Figure 4 but for a halo-finder linking length of $b = 0.15$. As expected, the discrepancies in the number of halos between the low and high resolution runs further worsen (Cf. the halo count vs. mass histogram, top right); the “orphaned” red spheres in the upper left plot all correspond again to smaller halos. But the overlinking problem is essentially absent.

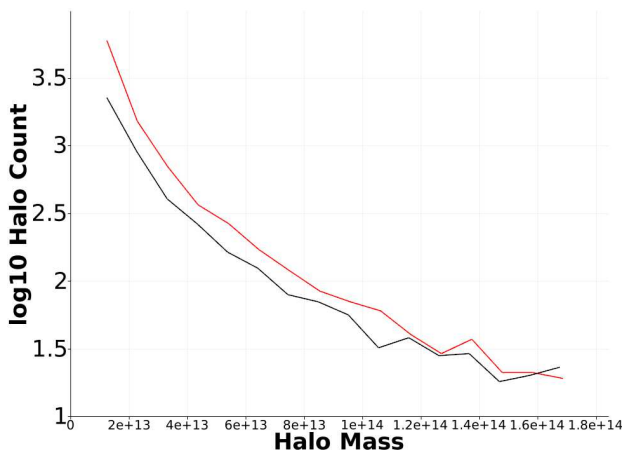


FIG. 6.— Number count of halos vs. mass for halos with less than 2500 particles. Black line: low resolution simulation, red line: high resolution simulation. Following our estimate, the low resolution simulation has fewer halos than the high resolution simulation over the whole mass range considered.

initial condition with 256^3 particles on a 256^3 grid at a starting redshift $z = 200$. We evolve these initial conditions with two different uniform force grids: a 256^3 grid and a 1024^3

grid. Therefore, the low resolution simulation has a force resolution of $\sim 1h^{-1}\text{Mpc}$ and the higher resolution simulation, of $\sim 250h^{-1}\text{kpc}$. (Note that because this is a demonstration problem, the chosen parameters are not representative of those actually used in full-scale simulations.) For each simulation we store the final timestep in the cosmo format which provides the positions and velocities of the particles. For the mass field we store the potential of each particle. These outputs can be readily read into ParaView and be analyzed.

3.2. The Analysis

In Heitmann et al. (2006) we derived a simple criterion for the force resolution required to resolve the mass and position of halos with a linking length $b = 0.2$ reliably. This criterion states that

$$\frac{\delta_f}{\Delta_p} < 0.62 \left[\frac{n_h \Omega(z)}{\Delta} \right]^{1/3}, \quad (3)$$

where δ_f is the force resolution (for a PM code, $\delta_f/\Delta_p = n_p/n_g$ with n_p being the cube root of the number of particles and n_g the cube root of the grid size), n_h the number of particles per halo, Δ the overdensity of interest measured with respect to the critical density, and Δ_p the particle separation. A nominal choice of $\Delta = 200$ corresponds roughly to a “virial

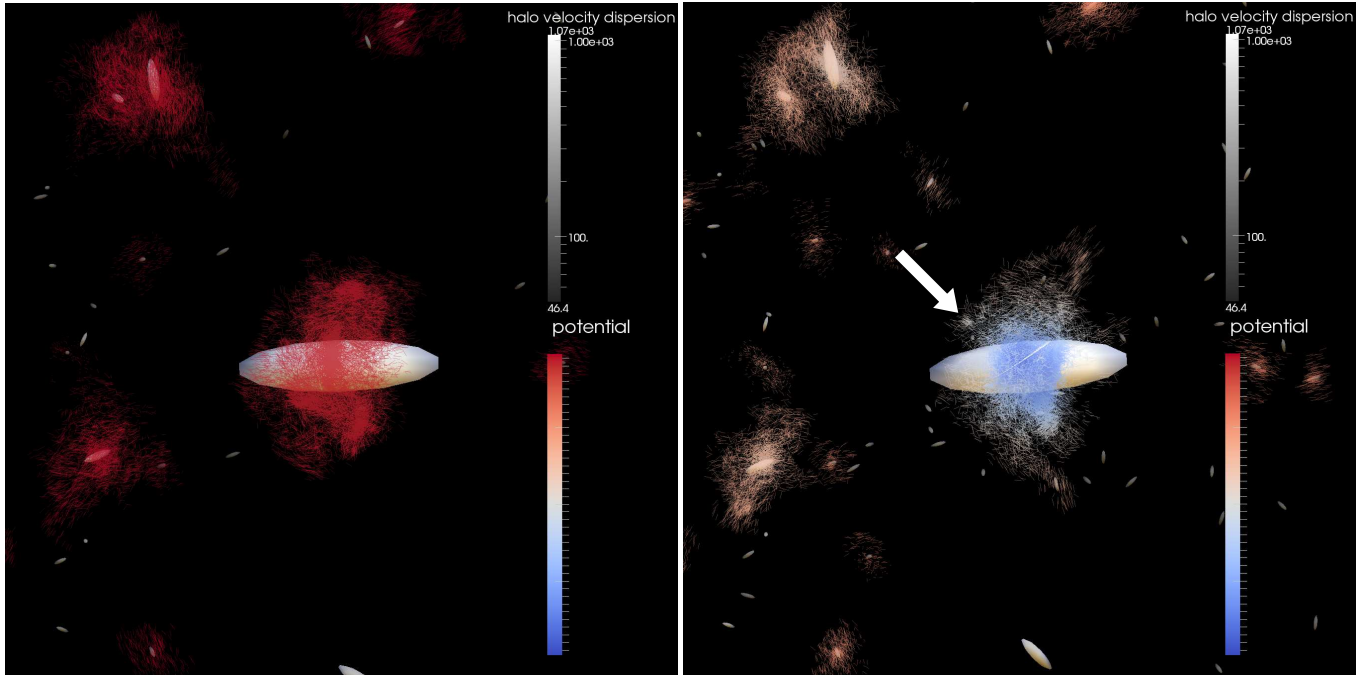


FIG. 7.— Visualization of one of the largest halos in the simulations: lower resolution (256^3 grid, left), higher resolution (1024^3 grid, right). Shown are the halos themselves (ellipsoids, oriented with respect to velocity and colored with respect to velocity dispersion measured in km/s) and particles within halos (within a $20 h^{-1}$ Mpc box centered around the major halo). The particles are represented by glyphs pointing in the velocity direction and colored with respect to their potential value (arbitrary units). Halos which do not show particles around them are outside the chosen $20 h^{-1}$ Mpc box. The white arrow in the right plot points at a small subhalo missing in the lower resolution simulation plot on the left.

mass”. With this choice, the criterion predicts that the 256^3 grid simulation should have sufficient resolution to capture halos with more than 3000 particles for $\Omega_m = 0.25$. This claim can be easily investigated with ParaView, and Figure 4 shows the results. We identify all halos with more than 3000 particles (linking length of $b = 0.2$) and show the particles that reside in halos for the different resolutions in a sub-volume. In addition, as a quantitative result, ParaView provides the overall number of halos found (116 for the high resolution run, 110 for the low resolution run) and we show a histogram of halo counts versus mass. This histogram indicates that the 5% discrepancy for the halo count is dominated by the smaller halos. The very convenient feature now is that once the analysis plot is set up as, e.g., shown in Figure 4, we can readily change the parameters for the halo finder and all panels will automatically show the new results. This makes the analysis task fast and convenient, allowing exploration of different settings in a simple manner. As an illustration, by changing the linking length to $b = 0.15$ in Figure 5, we find that the high resolution simulation now has 84 halos compared to 65 halos in the low resolution run, the difference between the two having increased to 20%. This is to be expected as it corresponds to an effective increase of Δ in the denominator of Eqn. (3), making the inequality harder to satisfy. If we lower the mass cut for the halos to 1000 particles per halo, we find, for $b = 0.15$, 487 halos in the high resolution run and 338 for the low resolution run, a difference of 30%.

Figure 6 (also created within ParaView) summarizes the results for halos with less than 2500 particles and a linking length of $b = 0.2$. The red line represents the halo counts as function of mass for the high resolution run, the black line the low resolution run. Over the entire mass range, the high resolution run has more halos.

As a next step we focus on a particular halo and investigate its structure as a function of force resolution. We choose the heaviest halo in the simulation that has no dominant substructure. The visualization of this halo and the quantitative information available from ParaView allows us to investigate the force resolution effects in more detail. First, we compare the basic properties of the ($b = 0.2$) halo from the two simulations: Table 2 summarizes the currently available halo properties as measured by ParaView. The halo from the low resolution simulation is slightly heavier, though the difference is below the percent level. The center of mass for both halos is also very close, and differences are again below 1%. The force resolution effects become more apparent for the velocity properties of the halos. The center of mass velocities differs at the 10% level and the high resolution halo has a larger velocity dispersion, by about 20%.

Next, we visualize the chosen halo and its surrounding region, as shown in Figure 7. To do this, we first identify all halos in the simulations with more than 100 particles. We then focus on the halo of interest and select all the particles that reside in halos in a $20 h^{-1}$ Mpc box around the central halo. We zoom into the box while continuing to display halos which reside behind it. The particles are displayed as two-dimensional glyphs pointing in the velocity direction of the particle. In addition, they are colored with respect to their potential value – red corresponds to a shallow potential while blue corresponds to a deep potential. The color coding is the same in both figures for ease of comparison. In addition to the particles within the halos, we show the center of mass of each halo by an ellipsoid pointing in the direction of the center of mass velocity. The halos are colored by their measured velocity dispersion σ_v (lighter colors correspond to higher values for σ_v) and sized with respect to their mass. We therefore have the following

TABLE 2
BASIC HALO PROPERTIES

	Low resolution halo	High resolution halo
Mass [$10^{15} h^{-1} M_{\odot}$]	1.34406	1.34344
Center of Mass [$h^{-1} \text{Mpc}$]	(128.8, 85.5, 219.8)	(129.0, 85.6, 220.0)
CoM velocity [km/s]	(-218.7, -94.2, -369.5)	(-191.3, -82.1, -367.3)
σ_v [km/s]	795.06	1072.16

information about the halos depicted in this visualization: (i) the number of halos in a certain region; (ii) the masses of halos; (iii) their center of mass position and velocity; (iv) the halo velocity dispersions; (v) velocity and position information about particles within halos; (vi) the potential values of the halo particles.

The first, and obvious, result of the local comparison is that the lower resolution simulation has fewer halos overall. The next immediate observation is the much deeper potential well at the center of the high resolution central halo, as well as the deeper potentials in the small neighboring halos. This deeper potential will lead to a higher mass concentration in the center of the central halo. It is also clear that the higher resolution simulation shows more substructure, e.g., in the left upper part of the central halo the high resolution result shows the formation of a small subhalo (marked by the white arrow) which is absent in the low resolution run. Overall, there are more particles on the outskirts of the low resolution central halo; on the left side many more particles appear to stream in to the halo. Thus, at least for this halo – and consistent with the overall results – one may conclude that for massive halos, the two force resolution effects compensate each other and the halo mass remains robust. This result is also in good agreement with the findings of Heitmann et al. (2005, 2008) and Lukić et al. (2007). In those papers, the mass functions obtained with different codes were compared and good agreement established even though the force resolution in the codes differed by up to a factor of 10. In Bhattacharya et al. (2010) a more detailed study was carried out analyzing halo mass differences from different force resolution simulations. In that study, the difference in force resolution was much larger than here – two simulations with force resolutions different by a factor of 14 were compared and the effect on the high mass halos was found to be at 4%. Overall, these findings are encouraging with respect to obtaining accurate predictions for the cluster mass

function from moderate resolution simulations. This relaxation of the spatial dynamic range requirement is particularly useful for cluster simulations where a large volume is needed to get good statistics for the associated mass function.

4. CONCLUSION

In this paper we have introduced ParaView as a powerful and convenient visualization and analysis tool for large cosmological N -body simulations. ParaView is an open-source, parallel visualization platform that can carry out visualization and analysis tasks on desktops as well as on supercomputers. We have implemented new readers and filters into ParaView that are designed for easy and efficient analysis of cosmological simulations. These tools include parallel particle readers (cosmo and GADGET format are supported) and a very efficient halo finder. The underlying infrastructure for the cosmology filters is taken from our recent code developments for MC³. As the analysis code suite for MC³ evolves and matures, we will port the new developments to ParaView. Currently, a spherical overdensity halo finder and a sub-halo finder are under final development.

In this paper, we demonstrated the use of ParaView and its interface for analyzing and visualizing cosmological simulation with a few examples, focusing on the effects of force resolution on the halo mass function in the cluster regime. The strength of ParaView is the ability of summarizing a large number of attributes of the simulation in a compelling visualization and at the same time, allow for visualization-aided analysis – the availability of quantitative information, allied to the visualization itself. Together with manipulation and analysis tools such as a calculator and binning routines, we believe that ParaView will be a very valuable new tool for the cosmology community.

A special acknowledgment is due to supercomputing time awarded to us under the LANL Institutional Computing Initiative. Part of this research was supported by the DOE under contract W-7405-ENG-36. The authors acknowledge support from the LDRD program at Los Alamos National Laboratory.

APPENDIX

In this appendix we provide some usage tips on visualizing cosmological N -body simulations with ParaView. Figure 8 shows a screenshot of the ParaView GUI interface. The first step is to read the particle file of interest. If the filename ends in .cosmo the ParaView reader will automatically identify the file as cosmo format and choose the correct reader. If the ending is different, a menu will appear and the user can pick by hand which format the reader should use. Once the cosmo format is specified, the user needs to enter the box size, the number of particles in one dimension, and the overload length that should be used for the halo finder. In the screenshot, the particle file that was read in was called "particle_white_lg" as apparent from the left upper list. Once the file is read in, some information is readily available and can be accessed by using the Information tab (e.g. number of particles, minimum and maximum velocities and positions). The Display tab opens choices for displaying the particles – the default option under "Style" and then "Representation" is "Outline" which will simply draw a box around the whole particle distributions. Changing this option to "Points" (as is done in the figure) will display the actual particles. Some of the particle attributes can then be changed, e.g. the size and the color options. The "eye" next to the particles_white_lg can be activated or de-activated by clicking on it – in our example it is de-activated which means that we do not show all the particles from the simulation, as explained below.

Next, we can apply a filter to the data as shown in the upper part of the figure. In the example, we evoke the halo finder. As in the case of the particle reader, options appear under "Properties" so that the linking length, minimum number of particles per halo and overload length can be specified. The halo finder then generates two new output files, "Output-0" and "Output-1". The first file holds all particles with the additional information of the halo tag. Particles which are not in a halo have the tag -1. By using another filter, "threshold" and requesting only particles to be displayed with halo tags ≥ 0 , all particles in halos can be displayed.

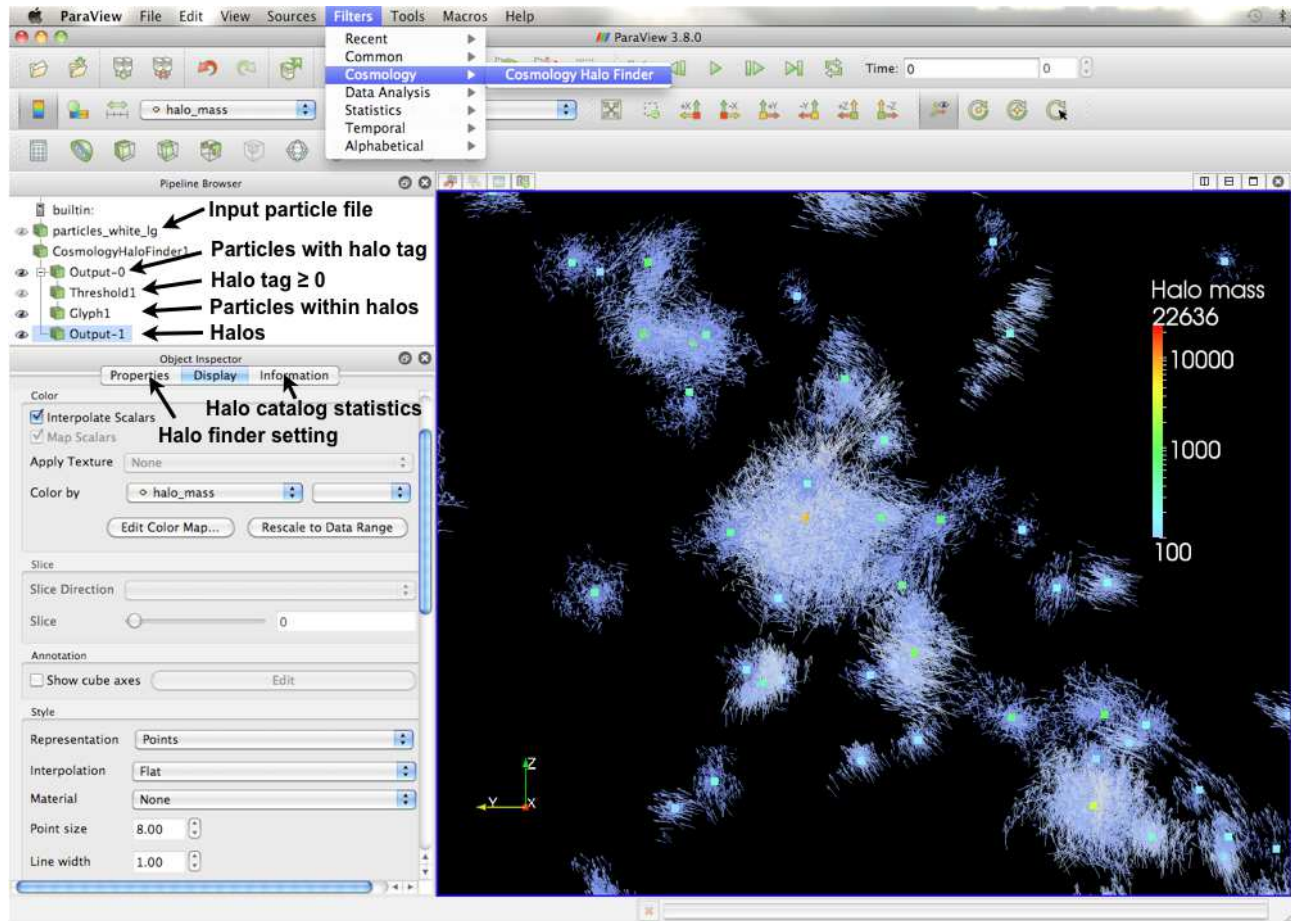


FIG. 8.— Screenshot of the ParaView GUI. Shown are particles within halos as two-dimensional glyphs and halo centers colored with respect to their mass. ParaView allows for easy changes in the properties of the displayed particles (in this case, e.g., linking length and minimum number of particles in a halo for the halo finder), properties of the visualization itself, such as color schemes, and quantitative information about the data set, e.g., maximum and minimum positions, velocities, and tags of particles or halo counts.

In the example, we decided to show these particles as two-dimensional arrows colored with respect to velocities. In order to do this, we used another filter “Glyphs” which allows for this option. As the activated eye next to “Glyph1” shows we are displaying these glyphs in the main window. “Output-1” contains the actual halo catalog. Again, by choosing “Information”, measurements of halo properties such as mass ranges and velocities will be shown. In the figure, “Output-1” is shaded in blue, which means the menu below can be manipulated for that output. In the current case, the halos are shown as points of size 8 colored with respect to mass.

REFERENCES

- Ahrens, J., Geveci, B., & Law, C. 2005, ParaView: An End-User Tool for Large Data Visualization. In the Visualization Handbook. Edited by Hansen, C.D. and Johnson, C.R. Elsevier.
- Bhattacharya, S., Heitmann, K., White, M., Wagner, C., Lukić, Z., & Habib, S. 2010, arXiv:1005.2239 [astro-ph.CO]
- Hsu, C.-H., Ahrens, J., & Heitmann, K. 2010, Pacific Visualization 2010
- Crocce, M., Fosalba, P., Castander, F.J., Gaztanaga, E. 2010, MNRAS, 403, 1353
- Cunha, C. & Evrard, A. 2010, Phys. Rev. D81, 083509
- Habib, S. et al. 2009, Journal of Physics: Conference Series, 180, 012019
- Heitmann, K., Lukić, Z., Habib, S., & Ricker, P. 2006, ApJ, 642, L85
- Heitmann, K., Ricker, P.M., Warren, M.S., & Habib, S. 2005, ApJS, 160, 28
- Heitmann, K. et al. 2008, Computational Science and Discovery, 1, 015003
- Heitmann, K., White, M., Wagner, C., Habib, S., & Higdon, D. 2010, ApJ, 715, 104
- Heitmann, K., Higdon, D., White, M., Habib, S., Williams, B., & Wagner, C. 2009, ApJ, 705, 156
- Kim, J., Park, C., Gott, III, R., Dubinski, J. 2008, ApJ, 701, 1547
- Lawrence, E., Heitmann, K., White, M., Higdon, D., Wagner, C., Habib, S., & Williams, B. 2010, ApJ, 713, 1322
- Lukić, Z., Reed, D., Habib, S., & Heitmann, K. 2009, ApJ 692, 217
- McBride, C. et al. 2010, in preparation; see also <http://lss.phy.vanderbilt.edu/lasdama/overview.html>
- Navarro, J., Frenk, C.S., & White, S.D.M. 1997, ApJ 490, 493
- Pope, A., Habib, S., Lukic, Z., Daniel, D., Fasel, P., Desai, N. & Heitmann, K. 2010, Computing in Science and Engineering 12, 17
- Schroeder, W.J., Martin, K.M., & Lorensen, W.E., 1996, The Visualization Toolkit: An Object Oriented Approach to 3D Graphics, Prentice Hall
- Springel, V. 2005, MNRAS, 364, 1105
- Summerfield, M. 2010, Advanced Qt Programming: Creating Great Software with C++ and Qt, Addison-Wesley
- Teyssier, R., Pires, S., Prunet, S., Aubert, D., Pichon, C., Amara, A., Benabed, K., Colombi, S., Refregier, A., & Starck, J.-L. 2009, A&A, 497, 335
- Warren, M.S., Abazajian, K., Holz, D.E., & Teodoro, L. 2006, ApJ 646, 881
- Wu, H.-Y., Zentner, A.R., & Wechsler, R.H. 2010, ApJ, 713, 856